Frequency-dependent reflectivity of shock-compressed xenon plasmas

H. Reinholz*
School of Physics, University of Western Australia, 35 Stirling Highway, Crawley, Western Australia 6009, Australia

Yu. Zaporoghets, V. Mintsev, and V. Fortov
Institute of Problems of Chemical Physics, Chernogolovka, Moscow Region 142432, Russia

I. Morozov
Institute for High Energy Densities of RAS, IHED-IVTAN, Izhorskaya 13/19, Moscow 127412, Russia

G. Röpke
FB Physik, University of Rostock, Universitätsplatz 3, D-18051 Rostock, Germany
(Received 23 February 2003; revised manuscript received 7 May 2003; published 26 September 2003)

Results for the reflection coefficient of shock-compressed dense xenon plasmas at pressures of 1.6–20 GPa and temperatures around 30 000 K using laser beams of wavelengths 1.06 μm and 0.694 μm are presented, which indicate metallic behavior at high densities. For the theoretical description of the experiments, a quantum statistical approach to the dielectric function is used. The comparison with molecular dynamics simulations is discussed. We conclude that reflectivity measurements at different wavelengths can provide information about the density profile of the shock wave front.

DOI: 10.1103/PhysRevE.68.036403 PACS number(s): 52.25.Mq, 05.30.Fk, 71.45.Gm, 52.27.Gr

I. INTRODUCTION

Recently, dense plasmas showing the transition from dielectric to metallic behavior were investigated extensively [1–4]. Highly compressed matter can be produced by shock waves from explosions or high-intense laser pulses. Heavy ion beams or *z*-pinch discharges are also used to create dense plasmas. For the diagnostics of properties in such highly compressed plasmas, optical measurements are most favorable, e.g., the reflectivity is expected to give information on the free-charge carrier density.

Reflectivity measurements under shock wave compression have been performed for different materials. For instance, Basko and co-workers [3] discussed experiments on Al and Si. Whereas the electron density is estimated to change at the shock wave front within a small interval of several nanometers, the change in temperature occurs within a layer of about 0.3 μm. Of high interest are recent experiments in liquid deuterium and water [4] which show a saturation of the reflectivity at values above 50%, indicating that a conducting state was attained.

We will consider xenon plasmas. In addition to former measurements of the reflectivity at a wavelength of 1.06 μm [1] results at the wavelength of 0.694 μm [2] are reported. At pressures in the region of 1.6–20 GPa and temperatures around 30 000 K a strong increase of the reflectivity has been observed indicating metallization.

In papers by Kurilenko and Berkovsky [5,6], the first series of experiments by Mintsev and Zaporoghets [1] was analyzed. The dielectric function was calculated via a dynamical collision frequency. The Born approximation was improved by including structure factor and local field corrections, but no consistent description of the measured reflectivities has been achieved. A different approach to the reflectivity was taken by Norman and co-workers [7,8], who proposed that the assumption of nonequilibrium excitations of plasma waves might provide a reasonable agreement with the experimental results. However, the structure of possible excitations of plasma waves in the shock wave front is an open question.

The detailed discussion of the reflectivity experiments requires a consistent theory for the frequency- and wave-number-dependent dielectric function. The application of the Drude model for a step-like shock wave front, as performed in Ref. [1], does not lead to a satisfying explanation of the experimental data. Improvements in evaluating the dielectric function [9], such as the dynamical and nonlocal behavior of the collision frequency, shows only minor effects in the reflectivity. In this paper, we will discuss a quantum statistical approach to the dielectric function as well as an alternative approach based on molecular dynamics (MD) simulations. An extended discussion of different effects, including the influence of the neutral particles, on the collision frequency will be presented. However, it will be shown that the use of the dielectric function in local thermodynamic equilibrium and the assumption of a sharp shock wave front are not appropriate to describe the experiments considered here.

In contrast to a step-like profile of the shock wave front, a more general approach would take into account the variation of the plasma parameters in space and time. Because of ionization processes the plasma formation exhibits a relaxation time so that the density profile of the free-charge carriers is considered to be spatially extended across the propagating shock wave front. In a recent paper [9], it was argued that the reflectivity data at 1.06 μm [1] can be interpreted assuming a finite width of the free-carrier density front profile. Having

*Fax +49 (0)381-498 2857. Email address: heidi@physics.uwa.edu.au

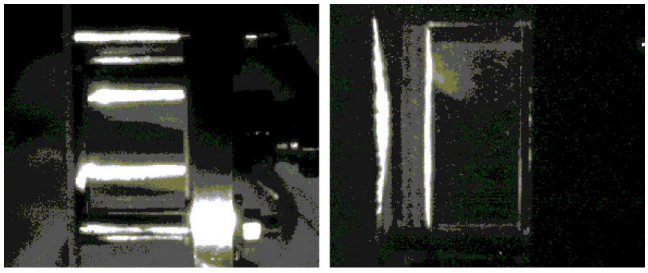

FIG. 1. Snapshots of the shock wave propagation in Xe. Left: initial gas cell. Right: 800 ns after entering the gas cell.

available experiments at two different wavelengths, it will be shown in this paper that the details of a density profile can be inferred more accurately. Possible further improvements of our approach will be discussed.

II. REFLECTIVITY MEASUREMENTS

To generate dense xenon plasma we used explosively driven shock waves which lead to compression and irreversible heating of the investigated gas. As the result of a detonation of high explosives a metal impactor is accelerated up to velocities of 5–6 km/s. The impactor runs into the bottom of the experimental vessel which is filled with xenon of an initial pressure of 2–5.7 MPa and produces an intense shock wave in the gas. For generating plasma at well-defined parameters it is necessary to produce plane and stationary shock waves. In order to control the spatial and temporal plasma slug parameters, the optical image of the shock wave in xenon was recorded by a PCO camera, see Fig. 1. In the left snapshot the initial gas cell view is shown. The gas cell was a 45×30-mm quartz cylinder. In the coordinate system of the snapshot the striker motion occurred from the left to the right. In the right snapshot, the shock wave front is shown 800 ns after the shock wave entered into the gas. The exposition time was 5 ns. The angle between the optical axis of the PCO camera and the plane of the shock wave front was about 5 deg. In this snapshot, the reflected shock wave in the air is also visible. For the diagnostics of plasma parameters, the 1.5 mm^2 area of the front shock wave was used. Good flatness and homogeneity of the plasma can be seen.

Two series of the experiments to measure the reflectivity of dense xenon plasma have been performed. In the earlier one [1], a laser beam with wavelength $\lambda=1.064$ μm was used. In the experiments reported here, a laser beam with wavelength $\lambda=0.694$ μm was chosen. The scheme of the experiment is shown in Fig. 2. The probe signal ($\tau_{\mathrm{imp}}=3\times10^{-8}$ s) was generated by the pulsed $Al_2O_3:Cr^{3+}$ laser system (1) with an electro-optical shutter based on a deuterated potassium dihydrophosphate (DKDP) crystal. In order to achieve the temporal stability, which is required for the diagnostic system, the special pump mode of the active laser medium was used. This has allowed to reduce the optical lock jitter value down to 6×10^{-9} s.

The computer control system (3) including the high-speed block of probe impulse delay adjustment, the high-speed–high-voltage electro-optical shutter key shapers, and the ionization gauges, located on the gas cell, ensured a synchronization of the probe impulse generation with the arrival of the shock wave front at the focal plane of the receiving optical unit. The timing bug did not exceed 6×10^{-8} s which corresponded to a deviation of the wave front from the optimum position at the moment of interaction with the laser impulse no more than 0.3 mm.

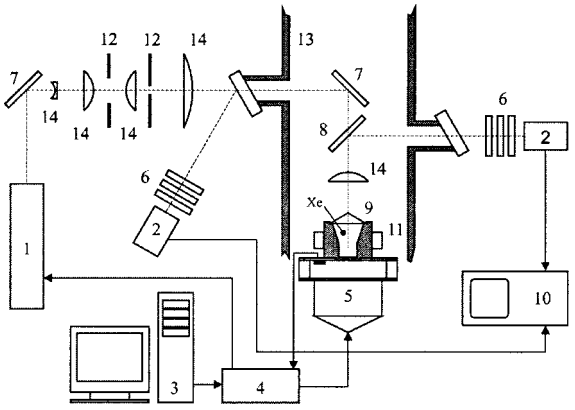

FIG. 2. Experimental setup. 1—$Al_2O_3:Cr^{3+}$ laser with electro-optical DKDP shutter, 2—photodetector, 3—control computer, 4—high-speed control block, 5—explosively driven generator, 6—interference filters, 7—mirror, 8—splitter, 9—axicon, 10—digititing oscilloscope, 11—gas cell with thermostat, 12—diaphragm, 13—explosive chamber, and 14—lens.

The first component of the receiving optical unit is a special axicon (9). Along the whole axicon caustic the condition for an adequate reception of a reflected signal was ensured. In order to decrease the level of false reflexes and to augment the receiving unit aperture angle, the axicon of the optical system of the reflected radiation reception was placed directly in the gas cell. The functioning of the optical receiving unit was checked by using static and low-speed dynamic objects with a well-known reflection coefficient.

The spatial characteristics of the probe radiation were shaped by employing a double telescopic cascade, in which nonspherical elements were also used. To minimize the error of the measurement, which is induced by instability and spatial heterogeneity of the transversal distribution of the probe radiation flux density, the optimization of the resonator in the $Al_2O_3:Cr^{3+}$ laser working in single-impulse mode was accomplished for Fresnel's index. The suppression of higher-order modes in the laser radiation was carried out, too. As a result, a precisely located spot of the probe radiation (spot diameter ≈1.5 mm) was formed at the focal plane of the receiving optical unit.

The intensity of the probe radiation was $\approx10^4$ W/cm^2. We investigated the influence of the probe radiation power on the reflective properties of the plasma. The reflection coefficient was also obtained while increasing the power by a factor of 7. The results coincided within the error limits of the measurement.

The registration of the radiation, reflected from the xenon plasma, was carried out by broadband photodetectors (2). The interference filters (6) with $\Delta\lambda=50$ Å were applied for

TABLE I. Experimental results [1] for the reflectivity R of xenon plasma at wavelength $\lambda_1 = 1.06$ μm and thermodynamic parameter values: pressure P, temperature T, mass density ρ, free-electron number density n_e, density of neutral atoms n_a, ionization degree $\alpha_{\mathrm{ion}} = n_e/(n_a + n_e)$, nonideality parameter Γ, and degeneracy parameter Θ.

P (GPa)	R^{exp}	T (K)	ρ (g cm^{-3})	n_e (cm^{-3})	n_a (cm^{-3})	α_{ion}	Γ	Θ
1.6	0.096	30 050	0.51	1.8×10^{21}	6.1×10^{20}	0.75	1.1	4.8
3.1	0.12	29 570	0.97	3.2×10^{21}	1.4×10^{21}	0.70	1.3	3.2
5.1	0.18	30 260	1.46	4.5×10^{21}	2.2×10^{21}	0.67	1.5	2.6
7.3	0.26	29 810	1.98	5.7×10^{21}	3.5×10^{21}	0.62	1.6	2.2
10.5	0.36	29250	2.70	7.1×10^{21}	5.4×10^{21}	0.57	1.8	1.9
16.7	0.47	28810	3.84	9.1×10^{21}	8.6×10^{21}	0.51	1.9	1.6

the selection of the spectral interval. The plasma reflection coefficient was determined from the ratio of the photodetector signal, which recorded the reflected radiation, and the photodetector signal, which fixed the probe impulse. The accuracy of the measured values of the reflection coefficient is better than 10%.

Before the experiment, the gas cell thermostatic control with an accuracy of ± 0.2 K was applied. In every experiment, the impactor velocity was measured with the electrocontact basis method ($u = 5.6$ km/s). The thermodynamic parameters of the plasma were determined from the measured shock wave velocity. The plasma composition was calculated within a chemical picture [10]. Working with a grand canonical ensemble [11] virial corrections have been taken into account due to charge-charge interactions (Debye approximation). Short range repulsion of heavy particles was considered within the framework of a soft sphere model.

In the parameter range of the shock wave experiments, derivations of up to 20% for the composition have been obtained depending on the approximations for the equation of state. This is within the accuracy of the experimental values of the reflectivity.

In accordance with these calculations, plasma densities of $\rho \approx 0.5$–4 g cm^{-3}, pressures of $P \approx 1.6$-20 GPa, and temperatures about $T \approx 3\times10^4$ K were realized during the experiments. Under these conditions the Coulomb interaction is characterized by the nonideality parameter $\Gamma = e^2(4\pi n_e/3)^{1/3}(4\pi\epsilon_0 k_B T)^{-1} = 1.1$–$1.9$. The results of the reflectivity measurements on dense xenon plasma at the wavelengths of $\lambda = 1.064$ μm and $\lambda = 0.694$ μm and the respective thermodynamic parameters are presented in Tables I and II, respectively. The parameter $\Theta = 2m_e k_B T(3\pi^2\hbar^3 n_e)^{-2/3}$, with m_e the electron mass, is the ratio of temperature and Fermi energy. The relative importance of quantum effects increases with Θ^{-1}.

III. DIELECTRIC FUNCTION IN DENSE PLASMA

A. Reflectivity

Assuming a step-like profile of the shock wave front, the laser beam reflection is determined by the electronic properties of the plasma behind the shock wave front. The reflection coefficient is given by [12]

$$R(\omega) = \left|\frac{1 - Z(\omega)}{1 + Z(\omega)}\right|^2 \tag{1}$$

with the surface impedance

$$Z(\omega) = -\frac{i\omega}{\pi c}\int_{-\infty}^{\infty} dk \frac{1}{k^2 - \omega^2 \epsilon_t(k,\omega)/c^2}, \tag{2}$$

where $\epsilon_t(k,\omega)$ is the transverse dielectric function depending on the wave number k and the frequency ω. The influence of the dependence on the wave number k has been investigated in Ref. [9] and found to be of insignificance at the parameter values of the considered experiments. As detailed below, only small values of k are relevant when performing the integration in the surface impedance. A comparison of the mean free path and the much larger skin depth also shows that nonlocal effects are not relevant here. Therefore, we take the long-wavelength limit of the dielectric function $\epsilon_t(0,\omega) = \epsilon(\omega)$ and find the Fresnel formula after performing the k integration,

$$R(\omega) = \left|\frac{\sqrt{\epsilon(\omega)} - 1}{\sqrt{\epsilon(\omega)} + 1}\right|^2. \tag{3}$$

The frequency ω has to be taken at the laser frequency, see Table III.

TABLE II. Experimental results [2] for the reflectivity R of xenon plasma at wave length $\lambda_2 = 0.694$ μm. Same notation for thermodynamic parameters as in Table I.

P (GPa)	R^{exp}	T (K)	ρ (g cm^{-3})	n_e (cm^{-3})	n_a (cm^{-3})	α_{ion}	Γ	Θ
4.1	0.11	33 000	1.1	3.8×10^{21}	1.3×10^{21}	0.75	1.3	3.2
9.1	0.18	32 000	2.2	6.6×10^{21}	3.6×10^{21}	0.65	1.6	2.1
20.0	0.43	29 000	4.1	8.8×10^{21}	9.9×10^{21}	0.47	1.9	1.6

TABLE III. Laser wavelength λ, frequency ω, and critical density $n_e^{\rm cr}$ (for explanation see text).

λ (μm)	ω (fs^{-1})	$n_e^{\rm cr}$ (cm^{-3})
0.694	2.72	2.35×10^{21}
1.060	1.78	1.02×10^{21}

If the relationship between the dielectric function and the thermodynamic parameters was known, the measurement of the reflectivity would provide information about, e.g., the particle density. Assuming the random phase approximation (RPA) for the dielectric function in the long-wavelength limit $\epsilon(\omega)=1-\omega_{\rm pl}^2/\omega^2$, with the plasma frequency $\omega_{\rm pl}=\sqrt{n_e e^2/(\epsilon_0 m_e)}$, a critical density $n_e^{\rm cr}$, see Table III, is obtained, at which the plasma frequency coincides with the frequency ω of the probing laser pulse. Total reflection occurs at densities higher than $n_e^{\rm cr}$ due to a negative dielectric function. However, by investigating the experimental data in Tables I and II, it is not possible to confirm such a direct relationship between the values of free-electron density n_e and the reflectivity R. The observed reflection coefficient increases smoothly with the free-electron density. It approaches only slowly the values characteristic for metals, although the critical density for metallic behavior is exceeded even at the lowest densities, see Table III. Taking collisions into account a reflectivity smaller than 1 is expected even in a metallic system. In the following, for the dielectric function beyond RPA, but preserving the assumption of a step-like shock wave front.

B. Dynamical collision frequency

In this section, we will evaluate the reflectivity formula (3) starting from a quantum statistical approach to the dielectric function within a linear response theory [13]. The complex frequency-dependent dielectric function

$$\epsilon(\omega)=1+\frac{i}{\epsilon_0\omega}\sigma(\omega)=1-\frac{\omega_{\rm pl}^2}{\omega[\omega+i\nu(\omega)]} \tag{4}$$

has been related to the dynamical conductivity $\sigma(\omega)$ or the dynamical collision frequency $\nu(\omega)$. This is identical with a generalized Drude formula [13]

$$\sigma(\omega)=\frac{\epsilon_0\omega_{\rm pl}^2}{\nu(\omega)-i\omega}, \tag{5}$$

where the dynamical collision frequency is defined microscopically and turns out to be a complex and frequency-dependent quantity. The commonly used phenomenological Drude formula follows if the collision frequency is taken in the static limit $\nu(0)=\epsilon_0\omega_{\rm pl}^2/\sigma_{\rm dc}$ relating it to the static (dc) conductivity $\sigma(0)=\sigma_{\rm dc}$.

We now consider the contributions from the free-charge carriers. The dynamical collision frequency can be evaluated in Born approximation with respect to the statically screened Coulomb potential (Debye potential), see Ref. [13]. In the nondegenerate case,

$$\nu^{ei,\rm Born}(\omega)=-i\frac{e^4\beta^{3/2}n_e}{24\sqrt{2}\pi^{5/2}\epsilon_0^2 m_e^{1/2}}\int_0^\infty dy\frac{y^3}{(\bar{n}+y^2)^2}\times\int_{-\infty}^{\infty}dx e^{-(x/y-y)^2}\frac{1-e^{-4x}}{x(x-\bar{\omega}-i\eta)}, \tag{6}$$

where

$$\bar{n}=\frac{\hbar^2 n_e e^2}{8\epsilon_0 m_e (k_B T)^2},\qquad \bar{\omega}=\frac{\hbar\omega}{4k_B T},$$

and the limit $\eta\to+0$ has to be taken. The second integral in Eq. (6) is a complex quantity,

$$\int_{-\infty}^{\infty}dx e^{-(x/y-y)^2}\frac{1-e^{-4x}}{x}\,{\rm P}\frac{1}{x-\bar{\omega}}+i\frac{\pi}{\bar{\omega}}e^{-(\bar{\omega}/y-y)^2}(1-e^{-4\bar{\omega}}).$$

Evaluating the collision frequency in the static limit ($\omega=0$), the result is the Ziman formula [14] applied to a Debye potential in the case of non-degeneracy,

$$\nu_{\rm dc}^{ei,\rm Born}=n_e\frac{e^4\beta^{3/2}}{6\sqrt{2}\pi^{3/2}\epsilon_0^2 m_e^{1/2}}\int_0^\infty dy\frac{y^3}{(\bar{n}+y^2)^2}e^{-y^2}. \tag{7}$$

The resulting values for the reflectivity calculated from the Drude formula (5) with the static collision frequency (7) are shown in Tables IV and V, together with the reflectivities resulting from the dynamical collision frequency in Born approximation (6) taken at the laser frequencies ω. Compared with the observed reflectivities, the results obtained from the static collision frequency in Born approximation do not show the strong increase in the reflectivity as a function of the electron density. The use of the dynamical conductivity in comparison to the static collision frequency increases the re-

TABLE IV. Reflectivities from step-like density profiles, calculated at the experimental parameter values for $\lambda_1=1.06$ μm. $R(\nu_{\rm dc}^{ei,\rm Born})$—Drude formula (5) with static collision frequency (7), $R(\nu^{ei,\rm Born}(\omega))$—dynamical collision frequency in Born approximation (6), $R_{\rm dc}^{\rm ERR}$—Drude formula (5) with static collision frequency (8), $R_{\rm dc}^{{\rm ERR},ea}$—Drude formula (5) with static collision frequency (8), and contribution of bound states to dielectric function, $R^{\rm MD}$—dielectric function (13) from Monte Carlo calculations.

P (GPa)	$R^{\rm exp}$	$R(\nu_{\rm dc}^{ei,\rm Born})$	$R(\nu^{ei,\rm Born}(\omega))$	$R_{\rm dc}^{\rm ERR}$	$R_{\rm dc}^{{\rm ERR},ea}$	$R^{\rm MD}$
1.6	0.096	0.272	0.304	0.502	0.452	0.27
3.1	0.12	0.342	0.351	0.588	0.531	0.50
5.1	0.18	0.381	0.380	0.630	0.572	0.59
7.3	0.26	0.404	0.399	0.661	0.593	0.60
10.5	0.36	0.429	0.419	0.692	0.616	0.67
16.7	0.47	0.457	0.447	0.729	0.646	0.68

TABLE V. Reflectivities from step-like density profiles, calculated at the experimental parameter values for $\lambda_1 = 0.694\ \mu$m. Same notation as in Table IV.

P (GPa)	R^{exp}	$R(\nu_{\mathrm{dc}}^{ei,\mathrm{Born}})$	$R(\nu^{ei,\mathrm{Born}}(\omega))$	$R_{\mathrm{dc}}^{\mathrm{ERR}}$	$R_{\mathrm{dc}}^{\mathrm{ERR},ea}$	R^{MD}
4.1	0.11	0.264	0.309	0.510	0.439	0.18
9.1	0.18	0.357	0.375	0.635	0.546	0.47
20.0	0.43	0.396	0.405	0.698	0.540	0.52

flectivity by about 15%, but it also fails to produce the steep dependence of the reflectivity on the electron density as observed in the experiment, see Table I. Similar results were obtained in Ref. [6] where a dynamical collision frequency in Born approximation was calculated using a pseudopotential for the electron-ion interaction and taking into account structure factor and local field corrections. However, these improvements do not lead to a qualitatively different behavior of the reflectivity.

The generalization of the dielectric function (4) to the nonlocal k dependent case is possible and has been considered in Refs. [13,15,16], using a Mermin ansatz. A comparison of results for the reflectivity (1) using in (2) a k dependent Born approximation for the collision frequency $\nu(k,\omega)$ in $\epsilon(k,\omega)$ and the Fresnel formula (3) with the frequency-dependent collision frequency in Born approximation (6) has shown deviations less than 5%. However, in general, the Born approximation is not appropriate in the region of plasma parameters under consideration, as pointed out, e.g., in Refs. [6,13]. Further improvements will be discussed in the following.

The Born approximation (Faber-Ziman result) underestimates the value of the dc conductivity. The correct low-density limit of σ_{dc} is given by the Spitzer formula and can be obtained considering strong collisions and using a renormalization factor as discussed in Ref. [13]. A constant correction factor following from the static limit was used in the case of small frequencies in Ref. [6]. On the other hand, screening of the interaction potential plays a role on a dynamical level which leads to the Lennard-Balescu scattering term. Taking these various limiting cases into account, an interpolation formula for the dc conductivity of a fully ionized Coulomb plasma was derived by Esser, Redmer, and Röpke [17],

$$\sigma_{\mathrm{dc}}^{\mathrm{ERR}} = a_0 T^{3/2}\left(1+\frac{b_1}{\Theta^{3/2}}\right)\left[D\ln(1+A+B)-C-\frac{b_2}{b_2+\Gamma\Theta}\right]^{-1}, \tag{8}$$

where T in K, σ in $(\Omega\,\mathrm{m})^{-1}$, and with the functions

$$A=\Gamma^{-3}\frac{1+a_4/\Gamma^2\Theta}{1+a_2/\Gamma^2\Theta+a_3/\Gamma^4\Theta^2}\times[a_1+c_1\ln(c_2\Gamma^{3/2}+1)]^2,$$

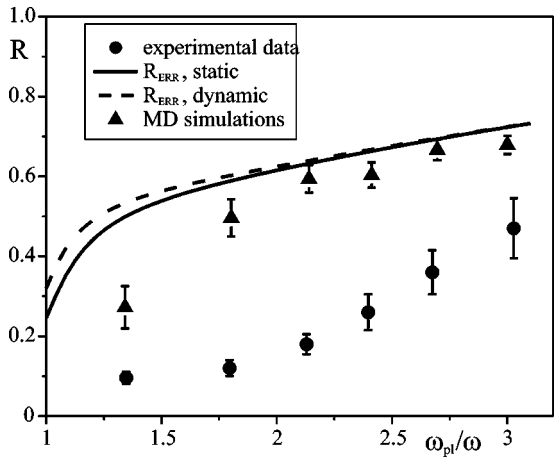

FIG. 3. Comparison of experiment with different theoretical approximations for reflectivity coefficient with probe laser of $\lambda_1 = 1.06\ \mu$m, assuming a step-like shock wave front.

$$B=\frac{b_3(1+c_3\Theta)}{\Gamma\Theta(1+c_3\Theta^{4/5})},$$

$$C=\frac{c_4}{\ln(1+\Gamma^{-1})+c_5\Gamma^2\Theta},\qquad D=\frac{\Gamma^3+a_5(1+a_6\Gamma^{3/2})}{\Gamma^3+a_5}.$$

The set of parameters is given by $a_0=0.030\,64$, $a_1=1.1590$, $a_2=0.698$, $a_3=0.4876$, $a_4=0.1748$, $a_5=0.1$, $a_6=0.258$, $b_1=1.95$, $b_2=2.88$, $b_3=3.6$, $c_1=1.5$, $c_2=6.2$, $c_3=0.3$, $c_4=0.35$, and $c_5=0.1$. They are fixed by the low-density expansion of the dc conductivity (Spitzer), the strong degenerate limit (Ziman) [14], and numerical data for the dc conductivity in the intermediate parameter region.

A comparison of this interpolation formula with experimental results was given in Ref. [17]. For the region of plasma parameters of interest, $1<\Gamma<2$ and $\Theta>1$, conductivities obtained from experiments have an accuracy of about 30% and can be reproduced by the interpolation formula. Another check of accuracy of the interpolation formula for the conductivity is given by MD simulations to be described below.

Using the Drude formula (5) with the collision frequency $\nu(0)$ from the conductivities $\sigma_{\mathrm{dc}}^{\mathrm{ERR}}$ we obtain the reflectivities $R_{\mathrm{dc}}^{\mathrm{ERR}}$. They are shown as $R_{\mathrm{dc}}^{\mathrm{ERR}}$ and R_{ERR},static in Tables IV and V, and Figs. 3 and 4, respectively. R_{ERR},dynamic in the figures denotes a dynamic approximation obtained from scaling the static result according to the Born case. The results for the reflectivities are up to 60% higher than the Born approximation, indicating that in contrast to the use of a dynamical collision frequency, which will change the reflectivity by about 10–15 %, the account of strong collisions in the collision frequency is more essential. Compared with the experimental results, the calculated reflectivities are too high, and the strong increase of the measured values with density cannot be explained.

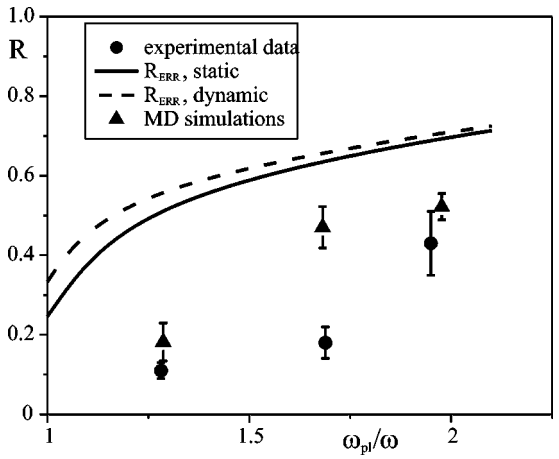

FIG. 4. Comparison of experiment with different theoretical approximations for reflectivity coefficient with probe laser of $\lambda_2 = 0.694\ \mu$m, assuming a step-like shock wave front.

C. Contribution of neutral components

The fraction of neutral particles in the plasma gives a contribution to the dielectric function which is not negligible. For high densities, this fraction increases to about 50%, see Tables I and II. Contributions due to additional scattering mechanisms of the free electrons with atoms as well as a direct contribution of the neutral component to the dielectric function should be taken into account in such a partially ionized system and will affect the reflectivity.

The scattering of free electrons on the atoms can be described by a screened polarization potential [18]

$$V_{\mathrm{p}}(r) = \frac{e^2}{4\pi\epsilon_0}\,\frac{\alpha_{\mathrm{p}}}{2(r^2+r_0^2)^2}\,e^{-2\kappa r}(1+\kappa r)^2, \tag{9}$$

with the polarizability $\alpha_{\mathrm{p}} = 27.3\,a_{\mathrm{B}}^3$ [19] for xenon and the screening parameter $\kappa^2 = 2n_e\beta e^2/\epsilon_0$. The cutoff parameter r_0 ensures the finite size of the polarization potential at small distances $r \to 0$ from the atom. It is caused by the finite extension of the atomic charge distribution so that the simple $1/r^4$ dependence is modified at short distances. According to the discussion in Ref. [15], the cutoff parameter was chosen to be the atomic radius $r_0 = 1$ Å $= 1.89 a_{\mathrm{B}}$ [19].

The electron-atom interaction leads to an additional contribution to the collision frequency in the following manner: $\nu = \nu^{ei} + \nu^{ea}$. In static Born approximation, the respective collision frequency is

$$\nu_{\mathrm{dc}}^{ea} = n_a \frac{e^4\beta^{3/2}}{6\sqrt{2}\,\pi^{3/2}\epsilon_0^2 m_e^{1/2}} \left(\frac{m_e \pi \alpha_{\mathrm{p}}}{\beta\hbar^2 r_0}\right)^2 \frac{1}{2} \times \int_0^\infty dy \frac{y^5}{(y+\kappa^2 l^2)^4} e^{-y-2r_0\sqrt{y}/l}, \tag{10}$$

where $l^2 = \beta\hbar^2/(8m_e)$. The strength of the electron-atom scattering is about one-third of that of the electron-ion scattering. Improving the Born approximation, the electron-atom collision frequency should be obtained from a *t*-matrix calculation, as has been done for the transport cross sections for xenon [20]. The inert gases show a typical Ramsauer minimum. However, at energies typical for the temperatures considered here, exploratory *t*-matrix calculations give larger collision frequencies compared to the Born approximation, which will be reduced if screening effects are taken into account.

The neutral component of the partially ionized plasma also gives an additional direct contribution to the dielectric function. According to a cluster expansion of the polarization function [21], several terms can be discussed. The main contribution comes from bound continuum transitions and can be approximated by

$$\epsilon^{ea}(\omega) = 4\pi\alpha_{\mathrm{p}} n_a \frac{1}{1-(\hbar\omega/E_0)^2}. \tag{11}$$

Both contributions to the dielectric function, Eq. (10) in the collision frequency as well as Eq. (11) have been taken into account in the calculation of the reflectivity, see row $R_{\mathrm{dc}}^{\mathrm{ERR},ea}$ in Tables IV and V. It leads to a reduction of the reflectivity by about 10% and increases with decreasing ionization degree.

Excited states may also contribute to the dielectric function. The lowest excited state occurs at about 8.3 eV above the ground state of $E_0 = -12.13$ eV. Its population is low at the considered temperatures of about 2.6 eV. Furthermore, considering the high densities which are near to condensed matter densities, the shift of the continuum of scattering states becomes quite large. Neglecting dynamical effects, an estimation is given by the Debye shift $-\kappa e^2/(4\pi\epsilon_0) = 36.2\ \mathrm{eV}/(\sqrt{\Gamma\Theta})$. It is reasonable to assume that the excited states have already merged into the continuum and should be included in the continuum contribution (11).

D. MD simulations

The analytical expressions used in the preceding section are valid for weakly coupled plasmas, $\Gamma \leqslant 1$. An alternative approach to obtain consistent results for the dielectric function also in the strong coupling region ($\Gamma \geqslant 1$) are MD simulations. We briefly outline the evaluation of the dielectric function and related quantities by MD simulations. A detailed discussion of the dynamical structure factor which is related to the dielectric function is given in Ref. [16]. Considerations of the long-wavelength limit which are relevant here can also be found in Ref. [22] and references given therein.

Within MD simulations, the normalized current-current correlation function [23]

$$K(t) = \frac{\langle \vec{J}(t)\cdot\vec{J}\rangle}{\langle J^2\rangle} \tag{12}$$

is obtained directly from the calculation of the total current of electrons $\vec{J}$ and then averaged over initial configurations of electrons and ions. This corresponds to the long-

wavelength limit $k \to 0$ of the k and ω dependent response function considered in Ref. [16].

The inverse of the dielectric function in the long-wavelength limit is related to $K(t)$ according to linear response theory [13],

$$\epsilon^{-1}(\omega) = 1 - i\frac{\omega_{\rm pl}}{\omega}\tilde{K}(\omega). \tag{13}$$

Here we introduced the complex Laplace transform of the normalized current-current correlation function (12)

$$\tilde{K}(\omega) = \lim_{\epsilon \to 0} \omega_{\rm pl} \int_0^\infty e^{i(\omega + i\epsilon)t} K(t)\, dt\,. \tag{14}$$

The complex dynamical collision frequency $\nu(\omega)$ can be derived from the generalized Drude formula (4) and expression (13):

$$\frac{\nu(\omega)}{\omega_{\rm pl}} = \frac{1}{\tilde{K}(\omega)} + i\left(\frac{\omega}{\omega_{\rm pl}} - \frac{\omega_{\rm pl}}{\omega}\right). \tag{15}$$

Agreement between MD simulations and the analytical approach to the collision frequency ν has already been found [16] for weakly coupled plasmas ($\Gamma \leqslant 2$) in the case of the dynamical structure function at finite wave numbers. Due to the quasiclassical limit and the use of an effective pseudopotential to account for quantum effects, the simulated data are not expected to give an exact result for the quantum current-current correlation function but have to be considered as a certain approximation. It is an open question whether the account for quantum effects by using a quasiclassical pseudopotential, as introduced for thermodynamic variables, is also justified in the case of kinetic properties. To take quantum effects into account more correctly one can perform wave packet molecular dynamics simulations [26].

We performed MD simulations which are based on the solution of the classical equations of motion. A finite system of 200 particles is considered and the average is taken over 1000 runs. We use a quasiclassical ''corrected Kelbg'' potential [24] in order to describe the interactions. This potential provides exact limiting values for the Slater sum and it's first derivative as the interparticle distance tends to zero. On the other hand, it avoids the formation of low energy bound states which cannot be treated within a quasiclassical approach. Thus we consider a two-component system of fully ionized singly charged particles. Such a model is applicable when the ionization degree is rather high and the degeneracy of electrons is almost negligible. The details of the simulation technique can be found in Ref. [25].

Exploratory calculations have been made for the long-wavelength limit and the results are encouraging. For example, the dc limit of the real part of $\tilde{K}(\omega)$ was evaluated for $\Gamma = 1.28$ and we found $\mathrm{Re}\,\tilde{K}(0) = \omega_{\rm pl}/\nu(0) = 5.1$. From the analytical calculation, using the interpolation formula (8) for the conductivity, the value $\mathrm{Re}\tilde{K}(0) = 4.64$ results for the same parameter values as for the simulations, the first line in Table II, which is in good agreement with the MD simulations result. For a more extended discussion, the accuracy of the MD simulations has to be improved, which will be the subject of a forthcoming work.

The results obtained for the reflectivity at a step-like density profile are collected in Figs. 3 and 4, where also experimental values are shown. The interpolation formula for conductivity (8) cannot explain satisfactorily the behavior of the measured reflectivity. The calculated values for the reflectivity are too high and show a smooth dependence on the density. This discrepancy cannot be removed by considering MD simulations which are not in contradiction with analytical calculations in the parameter region considered here, a fact which was found also in earlier investigations [16]. In conclusion, the measured strong increase of the reflectivity with the free-electron density is not reproduced assuming a step-like density profile.

IV. DENSITY PROFILE OF SHOCK WAVE FRONT

The spatial structure of the ionizing shock wave was already discussed in Ref. [1]. In the region of the shock wave front a steep increase of the free-electron density is expected. The width of the wave front is determined by relaxation processes in the plasma. In Ref. [1] it was estimated to be of the order of $d \approx 0.1$ μm, which is about one order of magnitude less than the laser wavelength. Preliminary calculations in a recent paper [9], which were based on the assumption that the density profile is linear within the shock wave front, found values for the thickness of the shock wave front in the order of 0.1–1 μm. This is in contrast to other systems such as metals [3] where free-charge carriers are already present, and not produced by ionization processes. Subsequently, the width of the wave front density profile is small.

If a density profile of the shock wave front is considered where the free-electron density smoothly increases from zero to its maximum value, the reflection of electromagnetic radiation occurs already in the outer region where the density is low. To perform an exploratory calculation, different density profiles were assumed where the electron density $n_e(z)$ increases with distance z from zero up to the saturation value n_e. The temperature is taken as a constant throughout the shock wave front. However, in a more refined approach, also a temperature profile $T(z)$ could be considered. It is also expected that the fraction of the neutral component would change within the shock wave front leading to a profile $n_a(z)$ which has been neglected so far.

A rigorous treatment of the propagation of laser radiation through a shock wave front should take into account the dependence of the collision frequency on the local electron density and the temperature. A precise result for the reflectivity from an arbitrary plasma front can be obtained from the direct solution of the equation for the electromagnetic field. Let us consider a planar wave propagating along z axis. Neglecting nonlocal effects for the conductivity we write the following Helmholtz equation for the complex amplitude of the electric field with frequency ω:

$$\frac{d^2E(z)}{dz^2} + 2\pi\epsilon(\omega, z)E(z) = 0, \tag{16}$$

where z is the distance in units of the wavelength. The function $\epsilon(\omega,z)$ has to be calculated for given density and temperature profiles $n_e(z)$, $T(z)$. In the local approximation the dielectric function $\epsilon(\omega,n_e(z))$ is considered to be dependent only on the local density. This approximation is justified here since the characteristic length of variation of $n_e(z)$ which is of the order of 1 μm is large compared with the microscopic correlation length which is in the order of the Debye radius of about 1 nm.

The appropriate solution of Eq. (16) is selected by taking the boundary condition

$$E(z_0)=E_0\ \exp\{-2\pi i z_0\sqrt{\epsilon(\omega,z_0)}\},$$

$$E'(z_0)=-2\pi i\sqrt{\epsilon_0(\omega,z_0)}E(z_0). \tag{17}$$

Then Eq. (16) is solved numerically starting from the initial point z_0. The reflectivity is given by [27]

$$R=\frac{|E_r(z_1)|^2}{|E_i(z_1)|^2}, \tag{18}$$

where

$$E_i(z)=\frac{1}{2}\left(E(z)-\frac{E'(z)}{2\pi i}\right)$$

and

$$E_r(z)=\frac{1}{2}\left(E(z)+\frac{E'(z)}{2\pi i}\right) \tag{19}$$

describe incident and reflected waves, respectively, and z_1 is taken at the free-space region $[\epsilon(\omega,z_1)=1]$.

In Ref. [9], we have considered a linear dependence of the electron density on the distance z within the shock wave front of width d_λ, $n_e(z)=n_e z/d_\lambda$ for $0\leqslant z\leqslant d_\lambda$, with n_e being the electron density behind the shock front. This is the simplest form to parametrize a density profile describing a finite width of the shock wave front, the index in d_λ refers to the wavelength at which the reflectivity was measured. For given density $n_e(z)$, the dielectric function $\epsilon(\omega,z)$ occurring in Eq. (16) was taken from the Drude formula (5) using the interpolation formula (8) for the dc conductivity $\sigma_{\rm dc}^{\rm ERR}$. Improvements considering the dynamical collision frequency and the contribution of neutral compounds, as discussed above, are expected to give only small modifications.

Determining the finite width d_λ of the shock wave front from the measured reflectivities presented above, the results for the different wavelengths $\lambda_1=1.06$ μm and $\lambda_2=0.694$ μm will differ from each other. The width of the plasma front seems to be thinner at higher frequencies. The laser beam with higher frequency can penetrate deeper into the density profile of the shock wave front. According to our parametrization, it measures a steeper gradient $dn_e(z)/dz=n_e/d_\lambda$ of the density profile. Therefore, it is necessary to investigate more flexible density profiles to perform the simultaneous parametrization of experiments at different laser frequencies. On the other hand, we conclude that the detailed density profile of the shock wave front may be inferred if measurements of the reflectivity at different laser wavelengths are performed.

In Ref. [15], we have considered Fermi-like density profiles given by $n_e(z)=n_e/(e^{z/l(n_e)}+1)$. While these are smoothly increasing we have chosen a more transparent parametrization of a density profile $n_e(z)$ which assumes two different density gradients. The results for the width of the shock wave front are effectively the same. The profile is given by two intervals with linear dependence on position,

$$n_e(z)=\begin{cases} n_e-\dfrac{n_e-n_0}{b_1(n_e)}z, & 0<z<b_1(n_e) \\ n_0\dfrac{b_1(n_e)+b_2(n_e)-z}{b_2(n_e)}, & b_1(n_e)<z<b_1(n_e)+b_2(n_e). \end{cases} \tag{20}$$

Here, parameter values which describe the experimental data at two different frequencies are $n_0=10^{21}$ cm^{-3}, $b_1(n_e)=(-0.025n_e^2+0.28n_e-0.18)$ μm, and $b_2(n_e)=(0.0072n_e^2-0.15n_e+1.25)$ μm. The densities have to be taken in units of 10^{21} cm^{-3}. Reflectivities are found which simultaneously describe the experimental data at two different frequencies quite reasonably in the density range considered.

Parametrization (20) gives the density profile $n_e(z)$ of the wave front in a smooth way in dependence on the maximum density n_e behind the front. Results are shown in Fig. 5. We conclude that by choosing appropriate values for the fit parameters the measured reflectivities can be reproduced within the error bars. The aim was to demonstrate that experimental reflectivities at different frequencies can be interpreted assuming a corresponding profile. In particular, we find that the density gradient is higher at higher densities.

It is of interest to show the consequences of the determination of the density profiles $n_e(z)$ which vary with the maximum pressure or maximum density n_e obtained behind the shock wave front, see Fig. 6. The corresponding curves for the reflectivity show a steep increase when n_e approaches the critical density $n_{\rm cr}$ for the respective laser frequencies. Then the reflectivity as a function of n_e remains nearly con-

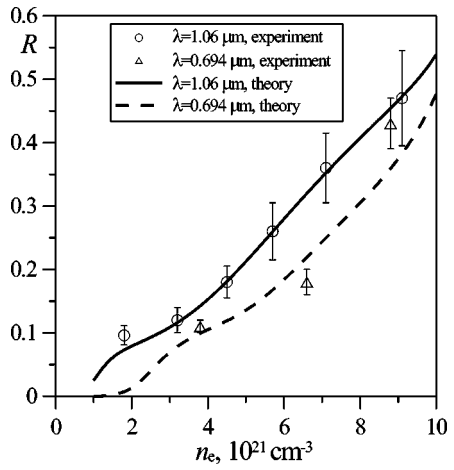

FIG. 5. Reflectivity coefficient depending on n_e in comparison to theory for a profile given by two intervals with linear dependence on the position according to Eq. (20).

stant, but rises once more at higher values of n_e. Here, d_λ as a function of n_e is decreasing. Possibly, the formation of the precursor ionization sheet is reduced if the velocity of the shock front is high. This should be discussed on the basis of a hydrodynamical code including ionization processes. Nonequilibrium processes may be of importance in order to describe the formation of free carriers.

Measurements at different frequencies show a bending of the density profile, from a sharp decrease near the shock front to a moderate decay at larger distances. Such a structure was also assumed in Ref. [1]. The dependence of the density profile on the maximum pressure or maximum density n_e obtained behind the shock wave front is of interest for further investigations. Note also that instead of the static conductivity we have to consider a dynamical one. However, as was shown for the step-like shock wave front, it is expected that the dynamical collision frequency leads to only minor modifications.

Compared with the value given in Ref. [1], our estimation of the width of the shock wave front comes out to be larger. We also observe a structure of the density profile, see Fig. 6.

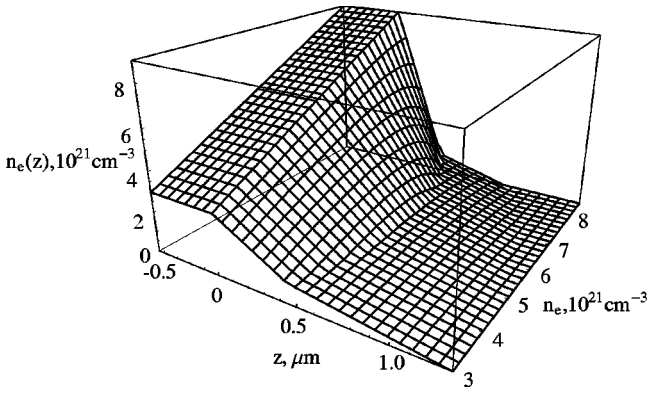

FIG. 6. Distribution of density of free electrons $n_e(z)$ in the shock wave front dependent on the electron density n_e (axis into the page) of the plasma bulk for a profile is given by two intervals with linear dependence on the position according to Eq. (20).

In a more sophisticated description, the temperature variation has to be considered as well as the variation of density of the neutral component. We can think about ionization processes due to heating in a precursor sheet in front of the shock wave and a steeper increase of the free-electron density at the shock wave. We have to include nonequilibrium processes given by the velocity of the wave front. Experiments at different wavelengths of the laser beam are important to get more information about the density profile of the shock front.

V. CONCLUSION

In order to infer plasma parameters from optical reflection coefficient measurements of dense xenon plasma produced in shock experiments, we have to take into account a finite width of the shock wave front of the order of 1 μm. Different forms of profiles $n_e(z)$ have been considered, and the reflectivity can be obtained by solving the Helmholtz equation.

Our calculations are based on an interpolation formula for the dc conductivity, obtained from a systematic quantum statistical treatment of different limiting cases. In particular, the account of the renormalization factor and of strong collisions is essential to obtain the correct low-density limit for the dc conductivity. The uncertainty in using the interpolation formula increases for $\Gamma \geqslant 1$. The values of the plasma parameter Γ for dense xenon plasmas considered here are in the region $1<\Gamma<2$ and $5>\Theta>1.5$ for the degeneracy. Improving this approach by taking a dynamical collision frequency or even a nonlocal instead of the static one, only marginal modifications of the reflectivity are expected. An alternative approach is given by MD simulations, which have been performed for classical model plasmas where the Coulomb interaction is replaced by a pseudopotential.

Xenon under the conditions considered is a partially ionized plasma. The composition is shown in Table I. The conductivity as well as the related quantities are influenced by the neutral component, which lead to a modification of the reflection coefficient. However, we find that neither analytical expressions for the collision frequency (static or dynamic, local or nonlocal) nor MD simulations as well as the account of neutral components can explain satisfactorily the behavior of the measured reflectivity as long as a step-like front profile is assumed.

Instead of step-like density profiles which are not able to explain the measured reflectivities, smooth density profiles were considered. We have shown that the experimental values of the reflectivity at different frequencies allow one to determine the density profile. For this, the density profile was parametrized by a simple ansatz given by two intervals with linear dependence on the position, Eq. (20), containing two parameters, which were given as a smooth function of the electron density in the shock wave fitting the measured reflectivities in the considered region. It has been found that the gradient of the density profile is higher for higher densities, i.e., closer to the step-like shock wave front. In order to explain the smooth density profiles, the propagation of a shock wave should be considered within a nonequilibrium

approach containing ionization and compression processes. The treatment of ionization kinetics and the inclusion of possible further nonequilibrium processes is the subject of future work.

As discussed above, improvements of our exploratory calculations on the finite shock wave front are possible replacing the static collision frequency by a dynamical one and considering nonlocal effects, which are expected to give only marginal effects. The density profile of the free electrons can be further modified, and we can include different profiles for temperature and the neutral component. Further items which should be addressed are the accuracy in determining the composition, in particular the free-electron density, and the relevance of the assumption of local equilibrium.

ACKNOWLEDGMENTS

We would like to thank V. Gryaznov for providing the thermodynamical calculations. We acknowledge support from the DFG within the SPP 1053 ''Wechselwirkung intensiver Laserfelder mit Materie'' and the SFB 198 ''Kinetik partiell ionisierter Plasmen'' as well as via the Grant No. RFBR-DFG No 99-02-04018. I.M. acknowledges support via Grants Nos. RFBR No 00-02-16310 and 03-07-90272V, H.R. acknowledges financial support from DFG.

[1] V.B. Mintsev and Yu.B. Zaporoghets, Contrib. Plasma Phys. **29**, 493 (1989).

[2] Yu.B. Zaporoghets, V.B. Mintsev, V.K. Gryaznov, and V.E. Fortov, in *Physics of Extreme States of Matter*, edited by V.E. Fortov *et al.* (Inst. Probl. Chem. Phys. RAN, Chernogolovka, 2002), p. 188 (in Russian).

[3] Th. Löwer, V.N. Kondrashov, M. Basko, A. Kendl, J. Meyer-ter-Vehn, R. Sigel, and A. Ng, Phys. Rev. Lett. **80**, 4000 (1998); M. Basko, Th. Löwer, V.N. Kondrashov, A. Kendl, R. Sigel, and J. Meyer-ter-Vehn, Phys. Rev. E **56**, 1019 (1997).

[4] P.M. Celliers *et al.*, Phys. Rev. Lett. **84**, 5564 (2000); R. Cauble *et al.*, Contrib. Plasma Phys. **41**, 239 (2001).

[5] Yu.K. Kurilenko and M.A. Berkovsky, in *Transport and Optical Properties of Nonideal Plasma*, edited by G.A. Kobzev, I.T. Iakubov, and M.M. Popovich (Plenum, New York, 1995), pp. 270–274.

[6] M.A. Berkovsky, Yu.K. Kurilenko, and H.M. Milchberg, Phys. Fluids B **4**, 2423 (1992).

[7] A.S. Kaklyugin, G.E. Norman, and A.A. Valuev, in *Physics of Strongly Coupled Plasmas*, edited by W.D. Kraeft and M. Schlanges (World Scientific, Singapore, 1996), pp. 435–440.

[8] G.E. Norman and A.A. Valuev, in *Strongly Coupled Coulomb Systems*, edited by G. Kalman, M. Rommel, and K. Blagoev (Plenum Press, New York, 1998), pp. 103–116.

[9] H. Reinholz, G. Röpke, A. Wierling, V. Mintsev, and V. Gryaznov, Contrib. Plasma Phys. **43**, 3 (2003).

[10] W. Ebeling, Physica A **43**, 293 (1969); W. Ebeling, A. Foerster, V. Fortov, V.K. Gryaznov, and A. Polishchuk, *Thermophysical Properties of Hot Dense Plasmas* (Teubner, Stuttgart-Leipzig, 1991).

[11] A.A. Likalter, Zh. Eksp. Teor. Fiz. **56**, 240 (1969) [Sov. Phys. JETP **29**, 133 (1969).

[12] W. Rozmus, V.T. Tikhonchuk, and R. Cauble, Phys. Plasmas **3**, 360 (1996).

[13] H. Reinholz, R. Redmer, G. Röpke, and A. Wierling, Phys. Rev. E **62**, 5648 (2000).

[14] J.M. Ziman, Philos. Mag. **6**, 1013 (1961).

[15] H. Reinholz, G. Röpke, I. Morozov, V. Mintsev, Yu. Zaparoghets, V. Fortov, and A. Wierling, J. Phys. A **36**, 5991 (2003).

[16] A. Selchow, G. Röpke, A. Wierling, H. Reinholz, T. Pschiwul, and G. Zwicknagel, Phys. Rev. E **64**, 056410 (2001).

[17] A. Esser, R. Redmer, and G. Röpke, Contrib. Plasma Phys. **43**, 33 (2003).

[18] R. Redmer, Phys. Rep. **282**, 35 (1997).

[19] S. Fraga, J. Karwowski, and K.M.S. Saxena, *Handbook of Atomic Data* (Elsevier, Amsterdam, 1976).

[20] V.M. Atrazhev, I.V. Chernysheva, and T. Doke, Jpn. J. Appl. Phys., Part 1 **41**, 1572 (2002).

[21] W.-D. Kraeft, D. Kremp, and W. Ebeling, and G. Röpke, *Quantum Statistics of Charged Particle System* (Plenum, New York/Akademie Verlag, Berlin, 1986).

[22] J.-P. Hansen, in *Strongly Coupled Plasma Physics*, edited by F. J. Rogers and H.E. DeWitt (Plenum, New York, 1987), p. 111.

[23] J.-P. Hansen and I.R. McDonald, Phys. Rev. A **23**, 2041 (1981).

[24] W. Ebeling, G.E. Norman, A.A. Valuev, and I.R. Valuev, Contrib. Plasma Phys. **39**, 61 (1999).

[25] I.V. Morozov, G.E. Norman, and A.A. Valuev, Dokl. Akad. Nauk. **362**, 752 (1998) [Dokl. Phys. **43**, 608 (1998)].

[26] E.J. Heller, J. Chem. Phys. **62**, 1544 (1975); D. Klackow, C. Toepffer, and P.-G. Reinhard, *ibid.* **101**, 10 766 (1994).

[27] J. Lekner, *Theory of Reflection* (Martinus Nijhoff Publ., Dordrecht, 1987).